

Research Article

Study on the Dynamic Properties of Concrete under Freeze-Thaw Cycles and CT Fine View Damage

Liangting Wang ^{1,2}, Zhishan Zheng ^{1,2}, Zheng Xiahou ¹, Xijian Chao ²,
and Ming Xia ¹

¹School of Civil Engineering, Jiangxi University of Engineering, Xinyu 338000, China

²School of Big Data and Computer, Jiangxi University of Engineering, Xinyu 338000, China

Correspondence should be addressed to Liangting Wang; jsjxy@jxue.edu.cn

Received 1 September 2023; Revised 23 November 2023; Accepted 14 December 2023; Published 28 December 2023

Academic Editor: Ahmed Ibrahim

Copyright © 2023 Liangting Wang et al. This is an open access article distributed under the Creative Commons Attribution License, which permits unrestricted use, distribution, and reproduction in any medium, provided the original work is properly cited.

In order to study the dynamic mechanical properties of concrete under freeze-thaw cycles, uniaxial impact compression tests were conducted on concrete specimens with different number of freeze-thaw cycles (0, 25, 50, 75, and 100) using a 50 mm diameter split Hopkinson pressure bar (SHPB) test device at an impact air pressure of 0.4 MPa and combined with a CT scanning system to analyze the internal fissures of concrete specimens before and after freeze-thaw cycles. The results showed the following. (1) The concrete specimens were divided into linear elastic stage, plastic stage, and damage stage under the freeze-thaw cycle, and the macroscopic mechanical parameters of the specimens were weakened with the increase of the number of freeze-thaw cycles. (2) Freeze-thaw intensified the expansion and penetration of the internal fracture of the specimens, and the CT scan results showed that the internal fracture parameters of the concrete specimens were increased with the increase of the number of freeze-thaw cycles, and the structural characteristics of the internal fracture show gradually complex expansion and evolution characteristics. (3) The degree of damage was defined at the fine level, which increased with the number of freeze-thaw cycles, establishing an intrinsic link between the fine deterioration of concrete specimens and the loss of macroscopic parameters under freeze-thaw cycles. The results are of great significance to further elucidate the internal structural characteristics of concrete material damage under freeze-thaw conditions and to reveal the damage deterioration mechanism.

1. Introduction

The durability research of concrete is usually aimed at the concrete specimens with standard maintenance for 28 days. However, in the road construction in the seasonal freezing area of northwest China, the concrete structures not only have to withstand the deterioration caused by freezing and thawing, but also inevitably suffer the isodynamic load caused by construction blasting disturbance [1–3]. In this complex environment, the internal cracks in concrete are intensified and expanded, and the degree of damage is aggravated, which is macroscopically manifested as a decrease in the mechanical properties of concrete [4, 5], seriously affecting the durability of the use of the structure and posing a potential threat to the development of the subsequent performance of the concrete structure and its service life

[6, 7]. Therefore, it is of great significance to investigate the dynamic mechanical properties and damage change characteristics of concrete under freeze-thaw cycle conditions to predict the performance deterioration law of concrete under freeze-thaw and dynamic load disturbance.

The mechanical properties of concrete materials under freeze-thaw cycle conditions have been extensively studied. Tian et al. [8] studied the effect of freeze-thaw cycles on the deterioration mechanism of concrete and found that the modulus of elasticity and strength of the specimens were decreased with the increase of the number of freeze-thaw cycles. Song et al. [9] analyzed the effect of freeze-thaw cycles on the compressive strength and tensile strength of two kinds of concrete materials through compressive and tensile experiments on the full-graded and wet-screened concrete specimens under different freeze-thaw cycle times. Zou et al.

[5, 10] carried out an experimental study on the attenuation law of concrete splitting tensile properties and repetitive load resistance and other indexes after freeze-thaw cycle, and the results showed that the mechanical property indexes of concrete compressive strength and repetitive load resistance showed an accelerated trend of decreasing with the increase of the number of freeze-thaw cycles. Wang et al. [11] found that the compressive and tensile strength of regenerated concrete was reduced under freeze-thaw cycle, and the degree of deterioration was higher than that of ordinary concrete. Fan et al. [12] found that the compressive and flexural properties of specimens were decreased with freeze-thaw cycle in their study of the durability of rubberized concrete under freeze-thaw cycle. Zhang [13] investigated the dynamic mechanical properties of the rubber concrete under different number of freeze-thaw cycles and impact air pressure and found that the freeze-thaw action destroys the rubber concrete, and there is a significant strain rate effect on its dynamic parameters. Freeze-thaw cycle will have a deterioration effect on the mechanical properties of concrete, and some scholars have characterized the degree of damage from a macroscopic point of view. However, most of the research on the mechanical properties under the action of freeze-thaw cycle focus on the static aspect of concrete, and the concrete will be frequently subjected to dynamic loads, such as impact and vibration, during the design service life, and there are a lot of differences between the mechanical properties and the static loads. Also, the nature of the damage is due to the frost expansion effect of concrete dominated by freeze-thaw action [14], resulting in the further development of internal cracks in concrete and the increase in the degree of damage. In order to reveal the deterioration mechanism of the kinetic properties of concrete materials under the conditions of freeze-thaw cycle, it is necessary to analyze the damage characteristics of concrete under the action of freeze-thaw cycle from a fine perspective.

At present, the methods used by domestic and foreign researches for the material fine damage mainly include electron microscope scanning, nuclear magnetic resonance (NMR), and CT scanning [15]. Various types of scanning electron microscopy can observe the pore fissure morphology and size, but they cannot quantitatively express the pore parameters; nuclear magnetic resonance can quantitatively analyze the distribution of pore size, but the evaluation of the pore structure of the super-dense coal beds is still in the exploratory stage. In contrast, industrial CT scanning can quantitatively analyze the fine structure and the resolution can reach the nanometer level [16–18]. Therefore, it is widely used in experimental studies of the mechanical properties of materials with fine damage [19–21]. Ge et al. [22] obtained CT pictures of microfracture sprouting, development, expansion, and penetration under different load levels using self-developed special loading equipment matched with CT machine and explored the preliminary law of damage morphology and evolution during uniaxial and triaxial destructive deformation of coal rock. Wang et al. [23] conducted CT real-time loading scanning test on shale, and the test results showed that the sprouting and development of fissures were affected by the

influence of laminar structure. Zhu et al. [24] investigated the evolution of fine-scale damage of concrete under different loads based on CT scanning technology and grey scale covariance matrix theory and established a quantitative relationship between statistical eigenvalues and fine-scale damage variables. Qin et al. [25] used X-CT scanning results to statistically analyze the initial damage of concrete in dams and quantitatively described concrete defects with extreme values and exponential distributions. Dang et al. [26] combined CT images and fractal analysis methods to establish the relationship between concrete damage and fractal dimension and investigated the fractal characteristics of concrete cracks. Mao et al. [27] combined CT technology and digital body correlation method to obtain the displacement and strain fields reflecting the deformation characteristics of materials at different stress stages. The above studies showed that industrial CT scanning technology can accurately and completely characterize the damage characteristics, deformation damage mechanism, and damage degree of materials, which is an effective way to study the fine structure of materials.

This paper utilizes the split Hopkinson pressure bar (SHPB) experiment system with a diameter of 50 mm to carry out dynamic impact compression test on freeze-thawed concrete, researches the mechanical properties of concrete under impact load after freeze-thaw cycle, combines the CT scanning system to obtain the internal crack evolution law before and after freeze-thawing of concrete, elucidates the microscopic damage characteristics of concrete specimen under the action of freeze-thawing, and provides a certain theoretical basis for the design of concrete engineering.

2. Experiment

2.1. Experimental Systems and Principles

2.1.1. SHPB System. The split Hopkinson press bar (SHPB) test system is shown in Figure 1. The bullet, the incident bar, and the transmitted bar are 300, 2000, and 1500 mm in length, respectively, all with a diameter of 50 mm. The bullet strikes the incident bar with the aid of air pressure in the high pressure chamber to generate a stress wave, the specimen undergoes a dynamic compression process, and as the bar is an elastic bar, the voltage (strain) signal reflecting the stress process on the specimen is collected with the aid of strain gauges.

Figure 2 gives the force and deformation of a microelement in an elastic bar under impact loading. Assuming that the length-to-diameter ratio of the elastic bar is sufficiently large, the cross section of the bar remains planar during loading, so that the force and deformation relations of the microelement under dynamic loading P_d can be obtained as follows:

$$-\frac{\partial P_d}{\partial x} \Delta x = \rho A \Delta x \frac{\partial^2 u}{\partial t^2}, \quad (1)$$

where A is the cross-sectional area of the bar, ρ is the density of the bar, and u is the displacement of the microelement at x after the force.

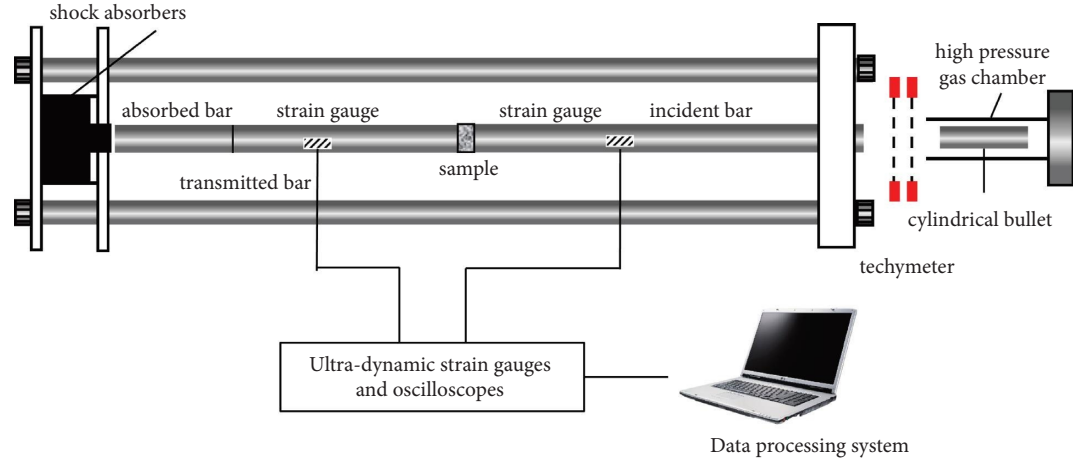


FIGURE 1: Schematic diagram of the SHPB system.

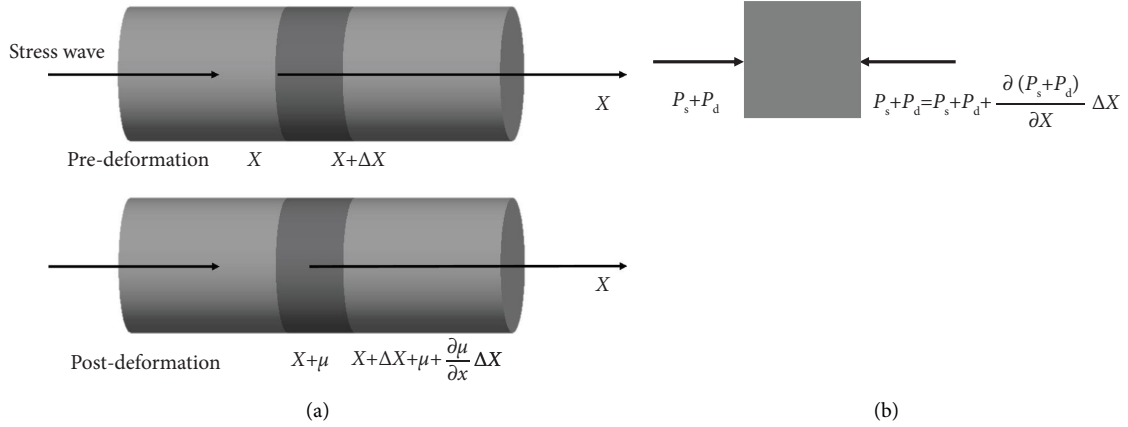


FIGURE 2: Schematic diagram of the impact test principle analysis. (a) Schematic diagram of elastic bar deformation. (b) Deformation diagram of a microelement in a bar under a stress wave.

According to the definitions of stress and strain and Hooke's law, it follows that

$$\begin{cases} \sigma = \frac{P_d}{A}, \\ \varepsilon = \frac{-\partial u}{\partial x}, \\ \sigma = E\varepsilon. \end{cases} \quad (2)$$

Combining equations (1) to (2), we get

$$\rho \frac{\partial^2 u}{\partial t^2} = E \frac{\partial^2 u}{\partial x^2}. \quad (3)$$

The principle of the SHPB test calculation is based on two basic assumptions [28]: ① one-dimensional stress wave assumption—the assumption that a one-dimensional stress wave propagates in a uniform elastic bar and ② uniformity assumption—the assumption that the stresses and strains in the specimen are uniformly distributed along the length

direction. Based on the incident strain $\varepsilon_i(t)$ and reflected strain $\varepsilon_r(t)$ measured by the strain gauges on the incident bar and the transmitted strain $\varepsilon_t(t)$ measured by the strain gauges on the transmitted bar, the stress, strain, and strain rate of the specimen during impact can be deduced from the following equations:

$$\begin{cases} \sigma(t) = \frac{EA}{A_0} \varepsilon_t(t), \\ \varepsilon(t) = -\frac{2C}{l_0} \int_0^t \varepsilon_r(t) dt, \\ \dot{\varepsilon}(t) = -\frac{2C}{l_0} \varepsilon_r(t), \end{cases} \quad (4)$$

where A , E , and C are the cross-sectional area (mm^2), modulus of elasticity (GPa), and longitudinal wave velocity (m/s) of the elastic compression bar, respectively, and A_0 and l_0 are the cross-sectional area (mm^2) and original length (mm) of the specimen, respectively.

2.1.2. CT Scanning Systems. The CT scan of freeze-thawed concrete was carried out with the aid of a microfocused computed tomography system, which was able to achieve an accuracy of 500 nm and met the requirements of this rock CT scan test. The scanning principle of the system is shown in Figure 3, the computer controls the radiation source to emit the beam, the X-ray passes through the object under test, the detector receives the attenuated signal, the CNC scanning platform carries the object under test and can be moved or rotated under computer control, the specimen rotates 360° with the turntable during the scanning process, the detector acquires the corresponding signal at certain angles and obtains a two-dimensional reconstructed image through mathematical transformation, the detector acquires the corresponding signal every certain Angle, and the two-dimensional reconstructed image is obtained by mathematical transformation. The flat panel detector is responsible for collecting the scanning data. The quantitative description of CT is CT number, which is converted to gray value according to a certain linear proportion. Since the linear attenuation coefficient of the material has an approximate correspondence with the density of the material, the CT image approximates the change in density within the material; finally, the X-ray in the device is a cone-beam ray, and for each scan, a multilayer CT image of the specimen in the ray area is obtained, each layer of the image has a certain scan thickness, and each pixel with thickness is called a voxel (Voxel), and the projection data collected by the computer through the 3D digital body image of the specimen can be obtained by computer reconstruction of the industrial CT slice image from the collected projection data.

2.2. Specimen Preparation and Experimental Protocol. The cement used in the experiment is P.O 42.5 cement produced by Conch Cement Co., Ltd., and its physical performance indexes are shown in Table 1; the fine aggregate is natural river sand, with the maximum particle size of 1.25 mm, the fineness modulus of 2.60, and the density of 2610 kg/m³; the coarse aggregate is selected from crushed stone with a particle size of less than 18 mm, and the water is tap water. According to the mass ratio of gravel : river sand : cement : water = 3.36 : 1.89 : 1 : 0.56[29], the concrete was poured with a size of $\phi 50 \times 25$ mm and maintained. After the curing was completed, freeze-thaw cycles and kinetic experiments were then carried out.

Firstly, the concrete specimens were subjected to freeze-thaw cycles, and in accordance with the requirements of the current standard “Test Methods for the Long-term Performance and Durability of Ordinary Concrete (GB/T50082-2009)” on the “fast-freezing method” for concrete, the specific test procedure and parameters of the freeze-thaw process were set as follows: (1) the number of freeze-thaw cycles was set to 0, 25, 50, 75, and 100, respectively, and the specimens were numbered A~E in turn, three specimens in each group; (2) before the freeze-thaw cycle to maintain the specimens, after reaching the specified requirements, remove the concrete specimens, and then wipe the surface moisture of the specimens with a wet cloth, and carry out appearance inspection and size and quality determination; (3) put the concrete into the rapid freezing and thawing chassis, turn on the freezing

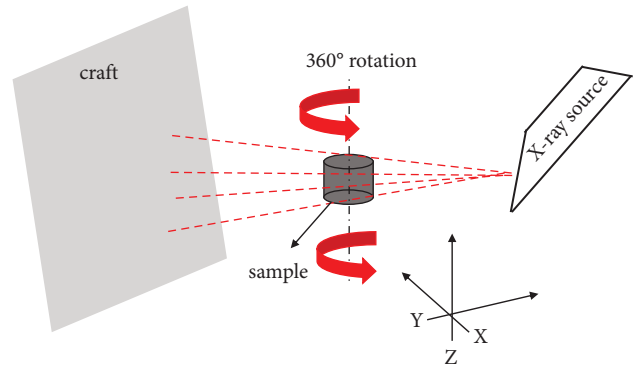


FIGURE 3: Basic principles of CT image acquisition.

TABLE 1: Cement physical property index.

Material	Solidification time (min)		Strength (MPa)	
	Initial setting time	Final setting time	3 d	28 d
Cement	≥45	≥390	≥17	≥42.5

and thawing tester to carry out the freezing and thawing cycle, the freezing time is controlled as 2 h, and the thawing time is controlled as 1.5 h. The rate of temperature change during the freezing and thawing cycle meets the following requirements: the time used to lower the central temperature of each specimen from 3°C to −16°C is about 80 min, while the time used to raise the central temperature of each specimen from −16°C to 3°C is about 50 min; the central temperature of the specimen during the test is shown in Figure 4.

Secondly, the concrete was scanned before and after the freeze-thaw cycle, and the internal damage before and after the freeze-thaw cycle was obtained by filtering, threshold segmentation, and three-dimensional reconstruction of the two-dimensional slices.

Finally, based on the SHPB experimental system, impact kinetic tests were carried out on concrete specimens with different number of freeze-thaw cycles, and test punches were made on the spare specimens before the tests. 0.40 MPa was selected as the impact air pressure according to the test punch results to obtain the kinetic properties of concrete under freeze-thaw cycles.

3. Experimental Results

3.1. Dynamic Stress-Strain Curves. The results of the stress waves at both ends of the specimen in the experiment are shown in Figure 5. It can be seen that the waveform curves corresponding to the sum of the transmitted strain and the incident and reflected strains overlap to a high degree, which meets the stress balance requirements of the test.

After checking the reliability of the test results, the stress-strain curve of the concrete specimen under impact loading can be calculated according to the calculation principle of the SHPB test. The stress-strain curves for different number of freeze-thaw cycles are shown in Figure 6. The change process is roughly divided into the following three stages: the first stage is the linear elastic stage, and the stress in this stage

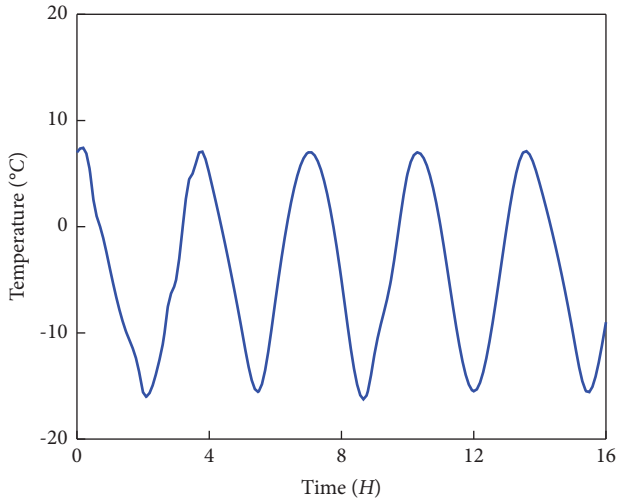


FIGURE 4: Variation of temperature with time in the rapid freeze-thaw tester.

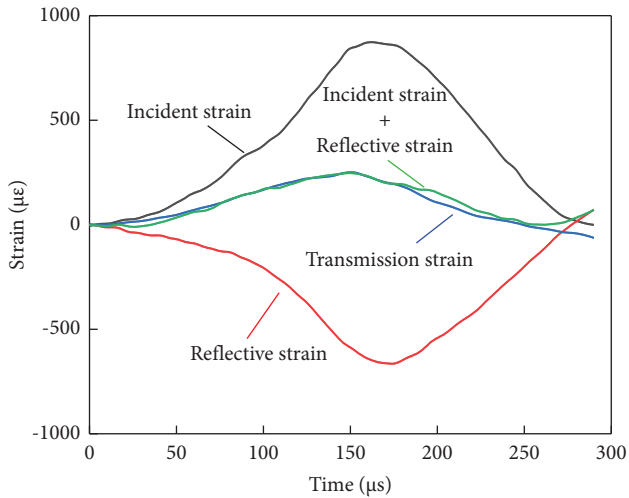


FIGURE 5: Dynamic stress balance curve for a typical specimen.

increases linearly with the increase of strain, this is due to the fact that the stress acting on the specimen is not sufficient to cause the crack in the specimen to expand and evolve or to produce new cracks, but only to keep the original crack in the specimen in a stable state or to produce a small value of expansion, with the elastic energy accumulating, but the elastic deformation of the specimen does not change qualitatively [30] and the slope remains basically unchanged, which can be taken as the dynamic elastic modulus of the specimen; the second stage is the plastic stage, the curve in this section is characterized by an upward convexity, the slope gradually decreases to 0 with the increase of stress, the specimen is subjected to impact load after the freeze-thaw cycle, the original cracks expand rapidly, sprouting a large number of new cracks and penetrating with the original cracks and eventually leading to the penetration of the specimen, the stress value at this time reaches the peak, i.e., the peak strength, and the corresponding strain is the peak strain; stage 3 is the damage stage, the slope of the curve is

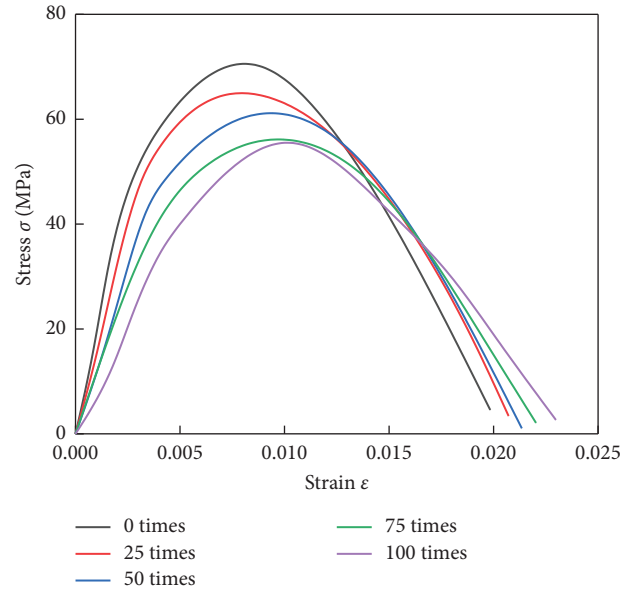


FIGURE 6: Stress-strain curves for different number of freeze-thaw cycles.

negative, the stress gradually decreases after the peak, the strain continues to increase, the specimen internal cracks gradually penetrate, macrocracks appear, and the bearing capacity gradually reduced. The analysis shows that as the number of freeze-thaw cycles increases, the slope of the peak strength and linear elastic phase of the stress-strain curve gradually decreases, while the strain corresponding to the peak strength gradually increases, indicating that the number of freeze-thaw cycles affects the dynamic properties of concrete specimens.

The macroscopic mechanical parameters (peak strength σ , peak strain ϵ , and modulus of elasticity E) of the specimens were obtained according to the stress-strain curves at different number of freeze-thaw cycles as follows (Table 2).

3.2. Macro-Mechanical Parameters of the Specimen

3.2.1. Peak Strength. In order to analyze the effect of the number of freeze-thaw cycles on the peak strength of the specimens, the relationship between the peak strength of the specimens and the number of freeze-thaw cycles is given in Figure 7. It can be seen that without freeze-thawing, the peak strength of the specimens ranged from 68.54 to 70.16 MPa, with an average value of 69.28 MPa; when the number of freeze-thaw cycles was 25, the peak strength of the specimens ranged from 63.89 to 65.04 MPa, with an average value of 64.42 MPa, which was 7.02% lower than that without freeze-thawing; when the number of freeze-thaw cycles was 50, the peak strength of the specimens ranged from 58.31 to 61.15 MPa, with an average value of 59.81 MPa, which is 13.67% lower than that without freeze-thaw; for 75 freeze-thaw cycles, the peak strength of the specimens was 56.12–58.86 MPa, with an average value of 57.39 MPa, which is 17.16% lower than that without freeze-thaw; for 100 freeze-thaw cycles, the peak strength of the specimens is

TABLE 2: Impact compression test results for concrete subjected to freeze-thaw cycles.

Number of freeze-thaw cycles	Specimen number	Peak strength (MPa)	Peak strength average value (MPa)	Peak strain	Peak strain average value	Modulus of elasticity (GPa)	Mean modulus of elasticity (GPa)
0	A1	70.16		0.00879		17.39	
	A2	68.54	69.28	0.00835	0.00852	17.11	17.13
	A3	69.15		0.00842		16.89	
25	B1	65.04		0.00944		15.78	
	B2	64.32	64.42	0.00911	0.00912	15.31	15.05
	B3	63.89		0.00880		14.06	
50	C1	58.31		0.0099		14.18	
	C2	61.15	59.81	0.00943	0.00965	12.54	13.28
	C3	59.97		0.00962		13.11	
75	D1	58.86		0.0110		11.51	
	D2	57.19	57.39	0.0102	0.01038	12.71	11.89
	D3	56.12		0.00994		11.45	
100	E1	56.09		0.01180		11.20	
	E2	55.47	55.81	0.01040	0.01103	10.98	10.70
	E3	55.87		0.01090		9.91	

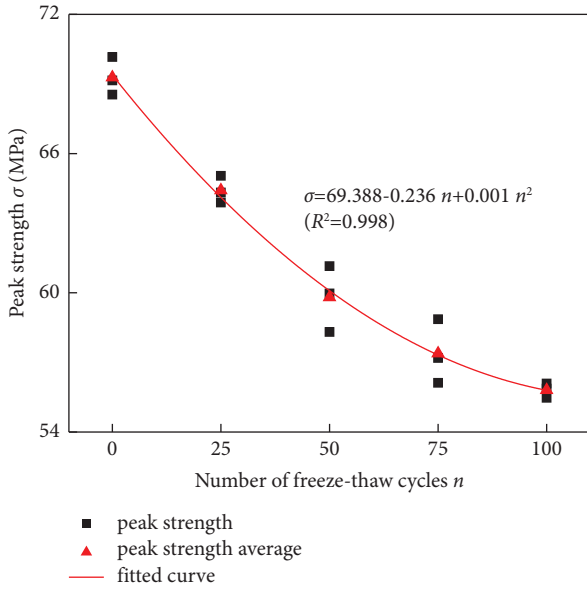


FIGURE 7: Peak strength versus number of freeze-thaw cycles.

55.47–56.09 MPa, with an average value of 55.81 MPa, which was 19.44% lower than that without freeze-thaw. From the fitting results, it can be seen that the peak strength of the specimens decreased as a quadratic function of the number of freeze-thaw cycles, indicating that the number of freeze-thaw cycles had a significant effect on the strength deterioration of the specimens.

3.2.2. Peak Strain. The variation curve of the peak strain ϵ_d with the number of freeze-thaw cycles is shown in Figure 8. With the increase in the number of freeze-thaw cycles, the peak strain of the specimen gradually decreased, and the average value of the peak strain increased from 0.00852 to 0.01103 as a quadratic function as the number of freeze-thaw cycles increased from 0 to 100, and the increase gradually increased, decreasing by 7.04%, 13.26%, 21.83%, and 29.46%, respectively, compared with the original specimen strength, which was due to damage caused by the expansion of internal cracks in the specimens after freeze-thaw cycles.

3.2.3. Dynamic Modulus of Elasticity. The dynamic modulus of elasticity is a macroscopic representation of the response of the internal microstructure of a material to an external load and a measure of its resistance to deformation. Figure 9 shows the variation of the dynamic modulus of elasticity of the specimens with the number of freeze-thaw cycles. It can be seen that the dynamic modulus of elasticity of the specimen gradually decreases with the increase of the number of freeze-thaw cycles, as follows: the average dynamic modulus of elasticity of the specimen is the largest without freeze-thaw cycles, 17.13 GPa; with the increase of the number of freeze-thaw cycles to 25, the average dynamic modulus of elasticity of the specimen decreases to 15.05 GPa, 87.57% of the original specimen; with the number of

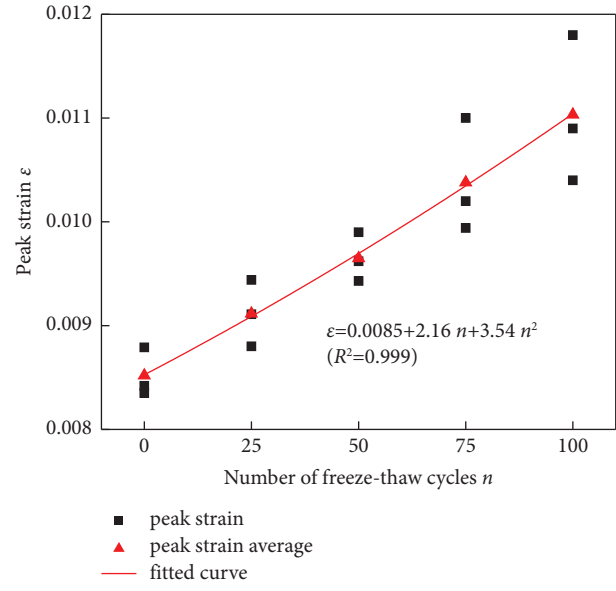


FIGURE 8: Peak strain versus number of freeze-thaw cycles.

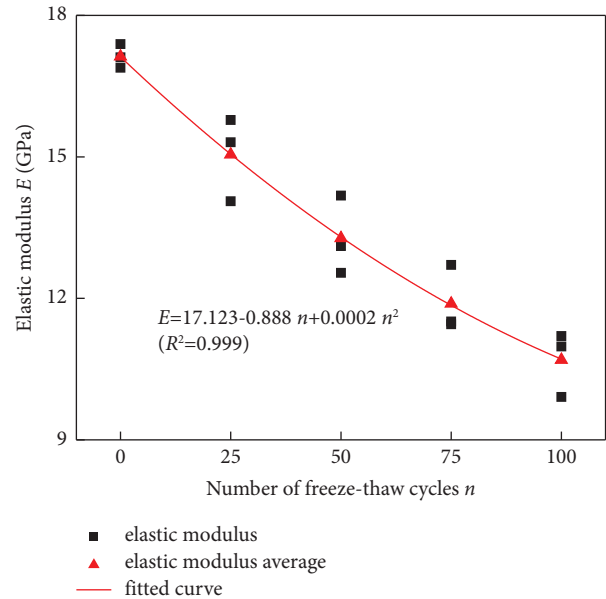
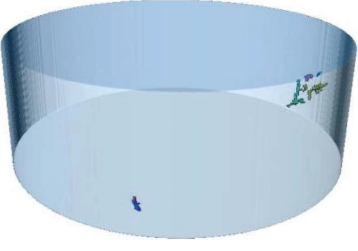
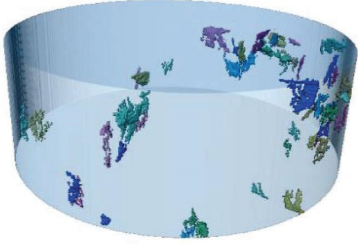
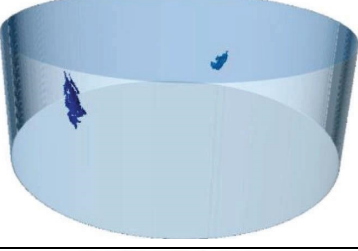
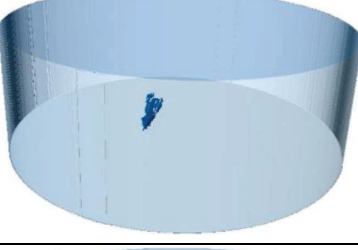
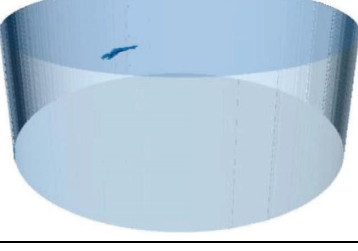
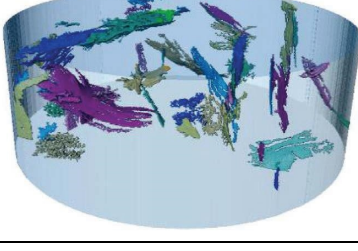


FIGURE 9: Dynamic modulus of elasticity versus number of freeze-thaw cycles.

freeze-thaw cycles further increased to 50, the average dynamic modulus of elasticity of the specimen decreased to 13.28 GPa, which is 77.52% of the original specimen; when the number of freeze-thaw cycles is increased to 75, the average dynamic modulus of elasticity of the specimen decreases to 11.89 GPa, which is 69.41% of the original specimen; when the number of freeze-thaw cycles is increased to 100, the average dynamic modulus of elasticity of the specimen decreased to 10.70 GPa, which is 62.46% of the original specimen. By fitting the two, it is found that the dynamic elastic modulus decreases approximately in a quadratic function with the increase of freeze-thaw cycles.

TABLE 3: CT scan images of concrete before and after freeze-thaw cycles.

Number of freeze-thaw cycles	Before freezing and thawing	After freezing and thawing
0		
25		
50		
75		
100		

3.3. A Closer Look at the Damage Characteristics

3.3.1. Fracture Extension Pattern. By reconstructing the CT scan results in three dimensions, the results of the reconstruction of the spatial distribution of the internal fracture structure of concrete before and after freezing and thawing are as follows (Table 3). The analysis shows that there were operational errors during the fabrication of the concrete, resulting in the existence of original microdefects of different sizes in the specimens before freeze-thawing. When the number of freeze-thaw cycles is 25, the specimens

were made more uniformly with fewer defects, but after the freeze-thaw cycles, the internal fissures sprouted and expanded; when the number of freeze-thaw cycles is 50, the specimens had natural original defects such as randomly distributed microfissures, and under the action of freeze-thaw, the internal fissures gradually grew and extended, and the initial fissure surface continuously expanded and evolved, and a new fissure close to penetration sprouted on the right side of the specimen. When the number of freeze-thaw cycles is 75 times and 100 times, the specimens have original defects; however, after the freeze-thaw cycles, the

TABLE 4: Internal fracture parameters of specimens at different number of freeze-thaw cycles.

Number of freeze-thaw cycles n	V (10^3 mm ³)	Before freezing and thawing			After freezing and thawing			ΔV (mm ³)	Δe (%)	ΔS (cm ²)
		V_1 (mm ³)	e_1 (%)	S_1 (cm ²)	V_2 (mm ³)	e_2 (%)	S_2 (cm ²)			
0	48.77	56.78	0.12	26.17	56.78	0.12	26.17	0	0	0
25	48.57	68.45	0.14	36.16	890.05	1.83	430.45	821.60	1.69	394.29
50	48.75	86.19	0.18	46.5	1007.23	2.07	536.1	921.04	1.89	489.60
75	49.50	40.36	0.08	23.99	1340.54	2.71	649.66	1300.18	2.63	625.67
100	49.19	20.45	0.04	13.58	1590.16	3.27	825.96	1569.71	3.23	812.38

internal fissures accelerated and evolved into many new fissures, which intersected each other. As the number of freeze-thaw cycles increases, the number of internal fractures increases, and the structural characteristics of the internal fractures show a gradually complex expansion and evolution, indicating that the erosion effect of freeze-thaw on the specimens is obvious.

To further investigate the effect of freeze-thaw on the internal fracture of the specimen, the internal fracture parameters (fracture volume V , fracture surface area S , and fracture rate e) were extracted, as shown in Table 4. After freeze-thaw, the crack volume, crack surface area, and crack rate of the sample all increased, which was due to the existence of primary cracks in the sample. Under the action of freeze-thaw, the internal cracks grew, developed and expanded, and interacted with the primary cracks to further form a network crack, resulting in internal damage of the specimen, and the crack volume, crack surface area, and crack rate increased significantly.

3.3.2. Concrete Damage Characteristics. Based on the internal fracture parameters of the specimen, the fracture expansion parameters were further calculated before and after the freeze-thaw cycles according to equation (5) [31] to analyze the damage of concrete before and after freeze-thawing.

$$\begin{cases} \Delta S = S_2 - S_1, \\ \Delta V = V_2 - V_1, \\ \Delta e = e_2 - e_1, \end{cases} \quad (5)$$

where ΔS is the incremental fracture surface area; ΔV is the incremental fracture volume; and Δe is the incremental fracture rate.

The results of the fracture extension parameters are shown in Table 4; with the increase of the number of freeze-thaw cycles, the increment of fracture surface area, fracture volume, and fracture rate of concrete specimens tended to increase. Compared with the nonfreeze-thaw condition, for specimens with 25 freeze-thaw cycles, ΔS , ΔV , and Δe increase by 394.29 cm², 821.60 mm³, and 1.69%, respectively. The increase was 489.60 cm², 921.01 mm³, and 1.89% at 50 times, 625.67 cm², 1300.18 mm³, and 2.63% at 75 times, and 812.38 cm², 1569.71 mm³, and 3.23% at 100 times, respectively.

To further evaluate the internal damage of concrete specimens after freezing cycles, the increment of crack rate is defined as the damage degree of specimen D [31, 32]. The

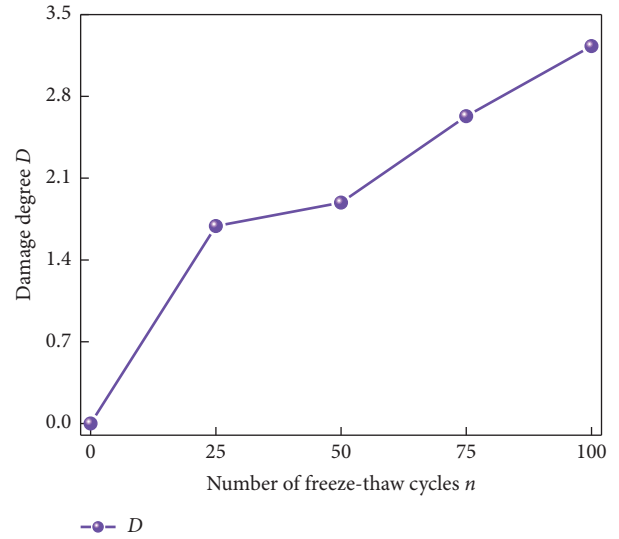


FIGURE 10: Relationship between the number of freeze-thaw cycles and the degree of damage.

damage degree of specimens under different number of freeze-thaw cycles is shown in Figure 10. As the number of freeze-thaw cycles increases, the degree of concrete damage increases and the increase gradually decreases. This is mainly due to the presence of a large amount of pore water inside the concrete specimen, which will produce volume expansion due to the freezing action [33]. It causes the expansion of the primary pores in the concrete, and the expansion of the water volume will generate stress inside the specimen, which will cause the internal cracks to expand. In the process of alternating positive and negative temperatures, a certain amount of tensile stress will be generated, causing fatigue damage to the concrete, and under the repeated action of freeze-thaw cycles, the pore cracks inside the specimen will continue to expand and the degree of damage will increase, thus causing the strength of the specimen to increase with the number of freeze-thaw cycles.

4. Conclusion

- (1) The dynamic stress-strain curves of concrete specimens under the action of freeze-thaw cycles had no obvious compression-density phase and were divided into linear elastic, plastic, and damage phases, and it was found that the peak strength, peak strain,

and elastic modulus of the specimens weakened as the number of freeze-thaw cycles increased.

- (2) Freezing and thawing intensified the expansion and penetration of internal cracks in the specimens, the results of CT scanning show that the number, volume, surface area, and fracture rate of internal cracks in the concrete specimens are found to increase with the number of freeze-thaw cycles, and the structural characteristics of the internal cracks showed a gradually complex expansion and evolution.
- (3) The porosity of concrete is affected by the number of freeze-thaw cycles, the increment of concrete crack rate increases with the number of freeze-thaw cycles, the degree of damage increases, the freeze-thaw action will cause fatigue damage to concrete, and with the increase in the number of freeze-thaw cycles, the increase in the degree of damage of the specimen decreases.

Data Availability

Data will be made available on request.

Conflicts of Interest

The authors declare that they have no conflicts of interest.

Authors' Contributions

Liangting Wang was responsible for thesis writing and modification. Zhishan Zheng and Zheng Xiahou were responsible for some experiments and data processing. Xijian Chao was responsible for some experiments and article polishing. Ming Xia was responsible for thesis typesetting.

Acknowledgments

This work was financially supported by Study on Freeze-Thaw Durability of Bidirectional Grid Reinforced Concrete Flooring Based on CT Scanning (GJJ2203016), Research on the Symbiosis Development and Governance Innovation of Platform Ecology under the New Development Pattern (22BJY101), and Research and Design of the Company's Human Resource Management System (GJJ2203012).

References

- [1] Z. L. Bai, B. X. Wang, and J. H. Lin, "Effect of freeze-thaw cycles on the bonding performance of basalt fiber woven mesh with concrete," *New Building Materials*, vol. 48, no. 9, pp. 36–40, 2021.
- [2] L. B. Wang and Z. Jun, "Study on the pore characteristics and dynamic mechanical properties of CFB ash concrete for road under the influence of seasonal freezing," *Journal of North China University of Water Resources and Hydropower (Natural Science Edition)*, pp. 1–8, 2023.
- [3] Y. F. Long, C. Pan, X. Q. Guo, and Y. W. Li, "Experimental study on dynamic mechanical properties of rubber concrete under freeze-thaw cycles," *Industrial Construction*, vol. 52, no. 4, pp. 163–170+139, 2022.
- [4] D. F. Cao, X. C. Qin, and S. F. Yuan, "Experimental study on the whole process of stressing prestressed concrete beams after freeze-thaw," *Journal of Civil Engineering*, vol. 46, no. 8, pp. 38–44, 2013.
- [5] C. Y. Zou, J. Zhao, F. Liang, and H. J. Ba, "Experimental study on stress-strain relationship of concrete under freeze-thaw environment," *Journal of Harbin Institute of Technology*, vol. 2, pp. 229–231, 2007.
- [6] A. Duan and J. R. Qian, "Experimental study on the full stress-strain curve of confined concrete under freeze-thaw conditions," *Journal of Rock Mechanics and Engineering*, vol. 29, no. S1, pp. 3015–3022, 2010.
- [7] A. J. Chen, Q. Zhang, J. Wang, and Z. F. Gai, "Freeze-thaw cycle tests and damage modeling of recycled concrete," *Engineering Mechanics*, vol. 26, no. 11, pp. 102–107, 2009.
- [8] W. Tian, K. Xing, and Y. L. Xie, "Mechanical experimental study on damage deterioration mechanism of concrete under freeze-thaw environment," *Experimental Mechanics*, vol. 30, no. 3, pp. 299–304, 2015.
- [9] Y. P. Song, X. J. Xu, and H. Liu, "Comparison of mechanical properties of fully-graded concrete and wet-screened concrete," *Shuili Xuebao*, vol. 43, no. 01, pp. 69–75, 2012.
- [10] C. Y. Zou, J. Zhao, F. Liang, J. L. Luo, and T. S. Xu, "Degradation of mechanical properties of concrete caused by freeze thaw action," *Journal of Building Structures*, vol. 29, no. 01, pp. 117–123, 2008.
- [11] C. X. Wang, D. Zhang, F. B. Cao, Y. X. Wu, C. Ye, and L. Li, "Research on mechanical properties and damage of recycled concrete after being subjected to freeze-thaw cycles," *Industrial Construction*, vol. 52, no. 05, pp. 199–207, 2022.
- [12] M. T. Fan and X. Wang, "Influence of the freezing and thawing cycle on the durability of rubber concrete," *Journal of Hubei University of Technology*, vol. 31, no. 04, pp. 101–104, 2016.
- [13] J. L. Zhang, "Investigations of dynamic mechanical performance of rubber concrete under freeze-thaw cycle damage," *Shock and Vibration*, vol. 2023, Article ID 6621439, 14 pages, 2023.
- [14] Z. P. Dong, X. K. Huang, Y. J. Lei, X. G. Liu, and D. T. Niu, "Research on frostheaving strain of stressed concrete under freeze-thaw cycle," *Journal of Xi'an University of Architecture and Technology*, vol. 55, no. 04, pp. 515–519, 2023.
- [15] L. Wang, H. Q. Liu, G. X. Xie, Q. P. Yuan, and L. P. Chen, "Fine characterization of the pore and fracture structure and strength degradation mechanism of gas bearing coal," *Rock and Soil Mechanics*, vol. 42, no. 12, pp. 3203–3216, 2021.
- [16] D. K. Wang, H. Zhang, J. P. Wei et al., "Dynamic evolution characteristics of gas-bearing coal fractures under the influence of gas pressure based on industrial CT scanning," *Journal of China Coal Society*, vol. 46, no. 11, pp. 3550–3564, 2021.
- [17] Y. T. Guo, C. H. Yang, C. G. Jia, J. B. Xu, L. Wang, and D. Li, "Research on physical simulation and fracture characterization methods for shale hydraulic fracturing," *Journal of Rock Mechanics and Engineering*, vol. 33, no. 1, pp. 52–59, 2014.
- [18] D. K. Wang, P. Zhang, H. Pu et al., "Experimental study on micro-CT of fracture structure evolution in coal bodies under temperature impact," *Journal of Rock Mechanics and Engineering*, vol. 37, no. 10, pp. 2243–2252, 2018.
- [19] Y. Jing, R. T. Armstrong, H. L. Ramandi, and P. Mostaghimi, "Coal cleat reconstruction using micro-computed tomography imaging," *Fuel*, vol. 181, no. 5, pp. 286–299, 2016.
- [20] J. P. Mathews, Q. P. Campbell, H. Xu, and P. Halleck, "A review of the application of X-ray computed tomography to the study of coal," *Fuel*, vol. 209, no. 4, pp. 10–24, 2017.

- [21] Y. B. Yao, D. M. Liu, Y. Che, D. Z. Tang, S. H. Tang, and W. H. Huang, "Non-destructive characterization of coal samples from China using microfocus X-ray computed tomography," *International Journal of Coal Geology*, vol. 80, no. 2, pp. 113–123, 2009.
- [22] X. R. Ge, J. X. Ren, Y. B. Pu, W. Ma, and Y. L. Zhu, "CT dynamic tests on the evolution of triaxial damage in coal rocks," *Journal of Rock Mechanics and Engineering*, vol. 5, pp. 497–502, 1999.
- [23] Y. Wang, Z. Q. Hou, and Y. Z. Hu, "In situ X-ray micro-CT for investigation of damage evolution in black shale under uniaxial compression," *Environmental Earth Sciences*, vol. 77, no. 20, pp. 717–812, 2018.
- [24] L. Zhu, F. N. Dang, W. H. Ding, Y. Xue, and L. Zhang, "Coupled X-ray computed tomography and grey level co-occurrence matrices theory as a method for detecting microscopic damage of concrete under different loads," *China Civil Engineering Journal*, vol. 53, no. 08, pp. 97–107, 2020.
- [25] X. Qin and Q. J. Xu, "Statistical analysis of initial defects between concrete layers of dam using X-ray computed tomography," *Construction and Building Materials*, vol. 125, pp. 1101–1113, 2016.
- [26] F. N. Dang, J. Y. Fang, and W. H. Ding, "Fractal comparison research of fracture of concrete samples under static and dynamic uniaxial tensile using CT," *Chinese Journal of Rock Mechanics and Engineering*, vol. 34, no. S1, pp. 2922–2928, 2015.
- [27] L. T. Mao, Z. X. Yuan, X. Y. Lian, R. D. Peng, and H. B. Liu, "Measurement of 3D strain field in red stone sample under uniaxial compression with computer tomography and digital volume correlation method," *Chinese Journal of Rock Mechanics and Engineering*, vol. 34, no. 01, pp. 21–30, 2015.
- [28] Z. D. Wei, *Experimental Study on the Effect of Gas deposit on Dynamic Mechanical Properties of Coal Body*, Anhui University of Technology, Huainan, China, 2018.
- [29] M. Li, X. B. Mao, L. L. Cao, R. R. Mao, and H. Pu, "Experimental study on the mechanical properties of coal under high strain rate," *Journal of Mining and Safety Engineering*, vol. 32, no. 2, pp. 317–324, 2015.
- [30] L. Zhu, *Study on Dynamic Mechanical Properties of Freeze-Thawed concrete by Hopkinson Pressure Bar*, Dalian University of Technology, Dalian, China, 2022.
- [31] L. Wang, L. P. Chen, H. Q. Liu et al., "Dynamic behaviors and deterioration characteristics of coal under different initial gas pressures," *Rock and Soil Mechanics*, vol. 44, no. 1, pp. 144–158, 2023.
- [32] W. Wang, X. Y. Liang, M. T. Zhang, Z. Y. Jia, S. Y. Zhang, and Q. Z. Wang, "Experimental study on failure mechanism and crack density of sandstone under combined dynamic and static loading," *Rock and Soil Mechanics*, vol. 42, no. 10, pp. 2647–2658, 2021.
- [33] M. Huang, Y. R. Zhao, S. H. Lin, and H. N. Wang, "Damage analysis of fracture performance of BFRPC under freeze-thaw cycles," *Concrete*, vol. 44, no. 12, pp. 31–35, 2021.